COMMUNICATIONS IN NUMERICAL METHODS IN ENGINEERING
Commun. Numer. Meth. Engng 2000; **00**:1–18 *Prepared using* cnmauth.cls *[Version: 2000/03/22 v1.0]*

P-wave and S-wave decomposition in boundary integral equation for plane elastodynamic problems

Emmanuel Perrey-Debain, Jon Trevelyan and Peter Bettess

School of Engineering, University of Durham, Science Laboratories, South Road, Durham, DH1 3LE Great Britain

SUMMARY

The method of plane wave basis functions, a subset of the method of Partition of Unity, has previously been applied successfully to finite element and boundary element models for the Helmholtz equation. In this paper we describe the extension of the method to problems of scattering of elastic waves. This problem is more complicated for two reasons. First, the governing equation is now a vector equation and second multiple wave speeds are present, for any given frequency. The formulation has therefore a number of novel features. A full development of the necessary theory is given. Results are presented for some classical problems in the scattering of elastic waves. They demonstrate the same features as those previously obtained for the Helmholtz equation, namely that for a given level of error far fewer degrees of freedom are required in the system matrix. The use of the plane wave basis promises to yield a considerable increase in efficiency over conventional boundary element formulations in elastodynamics. Copyright © 2000 John Wiley & Sons, Ltd.

KEY WORDS: elastodynamics, boundary integral equation, elastic wave scattering, plane wave basis

1. INTRODUCTION

In recent years a number of researchers have used a plane wave basis in conjunction with conventional element shape functions to develop improved formulations for the modelling of the Helmholtz equation. These methods fall into the category of Partition of Unity. Conventional shape functions are enriched by the presence of these plane wave functions. This makes the formation of the element matrices more complicated. However it has been found in general that many fewer degrees of freedom are needed for the solution of problems with a given level of error. One of the first publications to apply plane wave basis shape functions to finite elements for the Helmholtz equation was by Melenk and Babuška [1]. The first formulation of boundary

*Correspondence to: School of Engineering, University of Durham, Science Laboratories, South Road, Durham, DH1 3LE, Great Britain

Contract/grant sponsor: UK EPSRC (Engineering and Physical Sciences Research Council) grant numbers:; contract/grant number: GR/N09879 and SF/000169

Received 2002
Revised 2002

elements using this scheme was by de La Bourdonnaye [2]. The authors have recently applied these methods to the scalar Helmholtz wave equation [3, 4, 5]. In this paper we extend the technique to elasticity problems. At each node, as well as having a number of plane wave propagation directions, there are two different types of wave, the dilatation, or Pressure (P), wave and the distortional or Shear (S) wave.

2. INTEGRAL FORMULATION FOR TIME-HARMONIC PROBLEMS

The propagation of waves in an infinite elastic solid Ω' with Lamé constants μ, λ and density ρ in two-dimensional space is governed by the wave equation

$$\mu\nabla^2\boldsymbol{u} + (\lambda+\mu)\nabla\nabla\cdot\boldsymbol{u} + \omega^2\boldsymbol{u} = 0\,, \tag{1}$$

where the complex-valued displacement field $\boldsymbol{u}$ is assumed to have a time-dependence $e^{-\mathrm{i}\omega t}$, ω denotes the circular frequency and $\mathrm{i} = \sqrt{-1}$. The compressional wave number k_p and shear wave number k_s associated with the previous equation are

$$k_p = \omega\sqrt{\frac{\rho}{2\mu+\lambda}} \quad \text{and} \quad k_s = \omega\sqrt{\frac{\rho}{\mu}},$$

and we call κ the ratio between the shear and the longitudinal velocity, $\kappa = k_p/k_s$. In this paper, we are concerned with the radiation and the scattering of elastic waves by obstacles of arbitrary shape embedded in the propagative medium Ω'. The mathematical treatment of the scattering of an incident wave $\boldsymbol{u}^I$ by a simply connected bounded obstacle $\Omega \subset \Omega'$ of boundary line Γ (see Figure 1) leads to the boundary integral equation [6, 7, 8]

$$\boldsymbol{C}(\boldsymbol{x})\boldsymbol{u}(\boldsymbol{x}) + \int_\Gamma \boldsymbol{T}(\boldsymbol{x},\boldsymbol{y})\boldsymbol{u}(\boldsymbol{y})\,d\Gamma_y - \int_\Gamma \boldsymbol{U}(\boldsymbol{x},\boldsymbol{y})\boldsymbol{t}(\boldsymbol{y})\,d\Gamma_y = \boldsymbol{u}^I(\boldsymbol{x})\,, \tag{2}$$

where the first integral is taken in the sense of the Cauchy principal value. $\boldsymbol{U}$ and $\boldsymbol{T}$ are Stokes' displacement and traction tensors, respectively (see Appendix), which describe the fields at $\boldsymbol{y}$ due to a time-harmonic point force at $\boldsymbol{x}$ at frequency ω. $\boldsymbol{C}(\boldsymbol{x})$ is a geometric tensor associated with the location of the point $\boldsymbol{x}$ with respect to the boundary Γ. It has one of the following form: (i) the identity tensor $\boldsymbol{I}$ for $\boldsymbol{x}$ in Ω'; (ii) the zero tensor for $\boldsymbol{x}$ in Ω and (iii) a real symmetric tensor whose explicit expression can be found in [9] when $\boldsymbol{x}$ lies on the boundary Γ.

We are interested in problems where the obstacle Ω is characterized by a suitable prescription of surface traction $\boldsymbol{t}$ on Γ. Moreover, we consider a smooth boundary with a unique tangent at $\boldsymbol{x} \in \Gamma$, i.e. no edges or corners. The boundary value problem can then be written as

$$\frac{1}{2}\boldsymbol{u}(\boldsymbol{x}) + \int_\Gamma \boldsymbol{T}(\boldsymbol{x},\boldsymbol{y})\boldsymbol{u}(\boldsymbol{y})\,d\Gamma_y = \int_\Gamma \boldsymbol{U}(\boldsymbol{x},\boldsymbol{y})\boldsymbol{t}(\boldsymbol{y})\,d\Gamma_y + \boldsymbol{u}^I(\boldsymbol{x}) \quad , \quad \boldsymbol{x} \in \Gamma. \tag{3}$$

It is well known that the integral equation (3) has no unique solution at certain discrete frequencies. These frequencies coincide with the eigenvalues (or natural frequencies) of the corresponding interior problem. It is physically obvious that no resonance is possible in the external domain Ω' and therefore the above difficulty arises from the boundary formulation and not from the nature of a problem whose solution is unique. Various alternative formulations

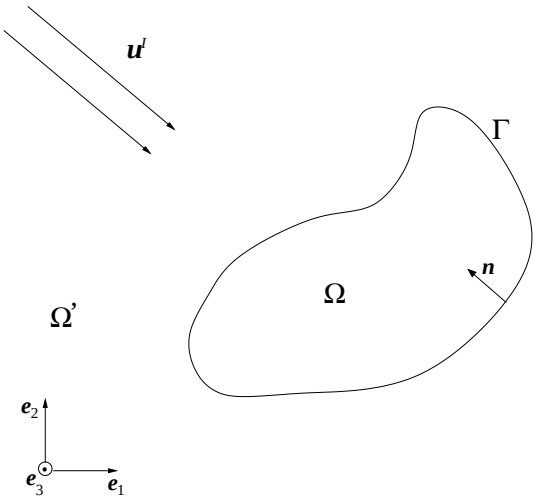

Figure 1. Scattering problem

of this exterior problem have been suggested to obtain an accurate solution at or near the eigenfrequencies [10]. Among them, the Combined Helmholtz Integral Equation Formulation (CHIEF) proposed by Schenck [11] has the advantage of being easier to implement and computationally less expensive than the other alternative methods. This formulation enforces the condition of zero displacement at points of the internal domain using the integral representation for those points. Let $\boldsymbol{x}^0_{i=1..N_0}$ be the so-called CHIEF points located in Ω. The additional constraints reads

$$\int_\Gamma \boldsymbol{T}(\boldsymbol{x}^0_i,\boldsymbol{y})\boldsymbol{u}(\boldsymbol{y})\,d\Gamma_y = \int_\Gamma \boldsymbol{U}(\boldsymbol{x}^0_i,\boldsymbol{y})\boldsymbol{t}(\boldsymbol{y})\,d\Gamma_y + \boldsymbol{u}^I(\boldsymbol{x}^0_i) \quad , \quad \boldsymbol{x}^0_i \in \Omega. \tag{4}$$

This formulation has the drawback that points falling on any nodal surface of the related interior problem do not provide linearly independent constraints. However, we shall assume in the sequel that we are not facing these unfortunate situations, though note that such situations are normally avoided by using multiple CHIEF points.

3. PRESENTATION OF THE FINITE ELEMENT BASIS

In this section, we shall propose a new finite element basis for the unknown displacement $\boldsymbol{u}$ in (3). To do so, let us recall that recent works carried out by the authors [3, 4, 5] concerning the Helmholtz problem showed drastic improvements when considering the unknown scalar potential as a finite sum of terms like $a_i(\boldsymbol{x})\exp[\mathrm{i}k\,\boldsymbol{\xi}_i\cdot\boldsymbol{x}]$ where the functions a_i are compactly supported on Γ and the vectors $\boldsymbol{\xi}_i$ describe the unit circle. This plane wave decomposition finds its justification in geometrical optics [2] and has been shown to be very efficient for sufficiently high wave numbers (say $ka > 50$ when the obstacle is a circular cylinder of radius a [4]). It is intuitively obvious that, under some appropriate modifications, such a representation should also be applicable to the wave equation (1). This becomes clearer when considering the

Helmholtz decomposition for the displacement field [12], namely

$$\boldsymbol{u} = \nabla\psi_p + \nabla \times (\psi_s \cdot \boldsymbol{e}_3)\,, \tag{5}$$

where the Lamé potentials ψ_p (resp. ψ_s) are the solution of the Helmholtz equation

$$\triangle\psi_p + k_p^2\psi_p = 0 \quad \text{and} \quad \triangle\psi_s + k_s^2\psi_s = 0. \tag{6}$$

For sufficiently high frequency, the potential ψ_p can be fairly approximated by a finite sum of terms like those introduced above with $k = k_p$ and similarly for ψ_s with $k = k_s$. Introducing these two plane wave approximations in (5) and keeping the leading order terms leads to the following representation

$$\boldsymbol{u}(\boldsymbol{x}) = \sum_i a_i^p(\boldsymbol{x})\boldsymbol{p}(\boldsymbol{x},\boldsymbol{\xi}_i) + \sum_i a_i^s(\boldsymbol{x})\boldsymbol{s}(\boldsymbol{x},\boldsymbol{\zeta}_i)\,,$$

where functions a_i^p and a_i^s are compactly supported on Γ and vectors $\boldsymbol{\xi}_i, \boldsymbol{\zeta}_i$ describe the unit circle. Fields $\boldsymbol{p}(\boldsymbol{x},\boldsymbol{\xi})$ and $\boldsymbol{s}(\boldsymbol{x},\boldsymbol{\zeta})$ stand respectively for the pressure wave (or P-wave) with direction $\boldsymbol{\xi}$ and the shear wave (or S-wave) with direction $\boldsymbol{\zeta}$, namely

$$\boldsymbol{p}(\boldsymbol{x},\boldsymbol{\xi}) = \boldsymbol{\xi}\exp[\mathrm{i}k_p\,\boldsymbol{\xi}\cdot\boldsymbol{x}]\,, \tag{7}$$

$$\boldsymbol{s}(\boldsymbol{x},\boldsymbol{\zeta}) = \boldsymbol{\zeta}^{\perp}\exp[\mathrm{i}k_s\,\boldsymbol{\zeta}\cdot\boldsymbol{x}]. \tag{8}$$

In this paper, functions a_i^p and a_i^s have been chosen to be the standard quadratic shape functions associated with the partition of the boundary

$$\Gamma = \bigcup_{n=1}^{N} \Gamma_n$$

where Γ_n is analytic and given by

$$\Gamma_n = \{\boldsymbol{x}(\eta) = (\gamma_1^n(\eta), \gamma_2^n(\eta)) : -1 \le \eta \le 1\}. \tag{9}$$

On each element, the displacement field is approximated as

$$\boldsymbol{u}(\boldsymbol{x}(\eta))|_{\Gamma_n} = \sum_{e=1}^{3}\sum_{l=1}^{M_p} \boldsymbol{a}_{e,l,n}^p(\boldsymbol{x}(\eta))u_{e,l,n}^p + \sum_{e=1}^{3}\sum_{l=1}^{M_s} \boldsymbol{a}_{e,l,n}^s(\boldsymbol{x}(\eta))u_{e,l,n}^s\,, \tag{10}$$

where the finite element basis $\boldsymbol{a}_{e,l,n}^p$ is the product of the quadratic Lagrangian polynomial N_e with a P-wave of direction $\boldsymbol{\xi}_l$ and similarly $\boldsymbol{a}_{e,l,n}^s$ is the product of the quadratic polynomial with a S-wave of direction $\boldsymbol{\zeta}_l$,

$$\boldsymbol{a}_{e,l,n}^p(\boldsymbol{x}(\eta)) = N_e(\eta)\boldsymbol{p}(\boldsymbol{x},\boldsymbol{\xi}_l)\,, \tag{11}$$

$$\boldsymbol{a}_{e,l,n}^s(\boldsymbol{x}(\eta)) = N_e(\eta)\boldsymbol{s}(\boldsymbol{x},\boldsymbol{\zeta}_l). \tag{12}$$

The terms $u_{e,l,n}^p$ and $u_{e,l,n}^s$ no longer represent the value of the displacement, but are instead the amplitudes of the set of P-waves and S-waves. Though other 'oscillatory' basis functions could be employed such as high order polynomials (Lagrangian, Legendre or B-Spline wavelets) or trigonometric-like bases (see for instance [13, 14], in the domain of structural dynamic

analysis), the specific feature of (10) is the physical meaning of such a decomposition. This latter point is discussed at the end of this section.

The continuity of $\boldsymbol{u}$ between two adjacent elements requires that

$$\boldsymbol{u}(\boldsymbol{x}(+1))|_{\Gamma_{n-1}} = \boldsymbol{u}(\boldsymbol{x}(-1))|_{\Gamma_n} \quad , \quad n = 1, \ldots, N \tag{13}$$

where the index 0 is assimilated with index N. It is easy to see that the following requirements

$$u^p_{3,l,n-1} = u^p_{1,l,n} \quad \text{and} \quad u^s_{3,l,n-1} = u^s_{1,l,n} \quad , \quad n = 1, \ldots, N \tag{14}$$

provide a sufficient condition satisfying (13). Now, in order to give a simple representation of $\boldsymbol{u}$ on the boundary Γ, it is convenient to group the set of indices e, l, n into a single index. To do this, let g^p be a one to one mapping from the set of integers $(e, l, n) \in [1, 2] \times [1, M_p] \times [1, N]$ to the single set $j \in [1, N^p_d]$ and similarly, g^s is a one to one mapping from the set of integers $[1, 2] \times [1, M_s] \times [1, N]$ to $[1, N^s_d]$. Here, N^p_d and N^s_d stand respectively for the number of degrees of freedom associated with the P-wave decomposition and the S-wave decomposition. We denote $N_d = N^p_d + N^s_d$ the total number of degrees of freedom of our problem. The field $\boldsymbol{u}$ on Γ can be then formally written as

$$\boldsymbol{u}(\boldsymbol{x}) = \sum_{j=1}^{N^p_d} \boldsymbol{q}^p_j(\boldsymbol{x}) u^p_j + \sum_{j=1}^{N^s_d} \boldsymbol{q}^s_j(\boldsymbol{x}) u^s_j \tag{15}$$

where functions $\boldsymbol{q}^p_j$ and $\boldsymbol{q}^s_j$ are defined as follows

$$\begin{array}{rcll} \boldsymbol{q}^p_j & = & \boldsymbol{a}^p_{1,l,n} + \boldsymbol{a}^p_{3,l,n-1} & , \quad j = g^p(1, l, n) \\ \boldsymbol{q}^p_j & = & \boldsymbol{a}^p_{2,l,n} & , \quad j = g^p(2, l, n) \\ \boldsymbol{q}^s_j & = & \boldsymbol{a}^s_{1,l,n} + \boldsymbol{a}^s_{3,l,n-1} & , \quad j = g^s(1, l, n) \\ \boldsymbol{q}^s_j & = & \boldsymbol{a}^s_{2,l,n} & , \quad j = g^s(2, l, n) \end{array}$$

and terms $u^p_{e,l,n}$ and $u^s_{e,l,n}$ have been respectively replaced by u^p_j and u^s_j. Though there is no restriction concerning the directions $\boldsymbol{\xi}_l$ and $\boldsymbol{\zeta}_l$, these are taken to be evenly distributed on the unit circle,

$$\begin{array}{rcll} \boldsymbol{\xi}_l & = & (\cos\alpha_l, \sin\alpha_l) & , \quad \alpha_l = 2\pi l / M_p \,, \\ \boldsymbol{\zeta}_l & = & (\cos\alpha_l, \sin\alpha_l) & , \quad \alpha_l = 2\pi l / M_s. \end{array}$$

An interesting feature of the approximation (10) is that it can be easily transformed into a conventional quadratic interpolation. It suffices to set $M_p = M_s = 1$ and consider the basis

$$\boldsymbol{a}^p_{e,1,n}(\boldsymbol{x}(\eta)) = N_e(\eta) \boldsymbol{e}_1 \,, \tag{16}$$

$$\boldsymbol{a}^s_{e,1,n}(\boldsymbol{x}(\eta)) = N_e(\eta) \boldsymbol{e}_2 \,, \tag{17}$$

where $\boldsymbol{e}_1$ and $\boldsymbol{e}_2$ provide the natural orthogonal basis of the plane as illustrated in figure 1. The approximation (10) then has the following form,

$$\boldsymbol{u}(\boldsymbol{x}(\eta))|_{\Gamma_n} = \sum_{e=1}^{3} N_e(\eta) \{ u^p_{e,1,n} \boldsymbol{e}_1 + u^s_{e,1,n} \boldsymbol{e}_2 \}. \tag{18}$$

This last expression is a quadratic approximation and for this particular case, coefficients $u^p_{e,1,n}$ and $u^s_{e,1,n}$ stand respectively for the horizontal and the vertical component of the displacement field $\boldsymbol{u}$ associated with node e and element Γ_n. This feature will allow a fair comparison between the usual polynomial interpolation and the new wave basis whatever the geometry of the curve Γ. Let us finish this section by mentioning that another justification for the use of the new finite element basis can be found in [1]. The approximation (10) is nothing else than the product of the standard shape functions with functions having good local approximation properties, i.e. functions that solve the differential equation. Indeed, the P-wave and S-wave are the only homogeneous plane waves solving (1) and, in a finite element method context, the representation (10) can be seen as a particular application of the Partition of Unity Finite Element Method.

4. NUMERICAL PROCEDURE

In very recent papers [3, 4], we found some success in solving the integral equation by using a direct collocation approach. The same technique will be used here. By considering the expression (10) and the additional requirements (14), it is straighforward to see that there are $2(M_p + M_s)$ number of degrees of freedom per element. Due to the vectorial nature of the displacement field, the collocation of (3) at a point $\boldsymbol{x}$ on the boundary Γ yields 2 independent equations. Therefore, the collocation of (3) at M_p+M_s different points located on each element leads to a square system. In this study, these points have been chosen arbitrarily to be evenly distributed in the parametric space along each element Γ_n as

$$\boldsymbol{x}_{i=g(e,m,n)} = (\gamma^n_1(\eta_{e,m}), \gamma^n_2(\eta_{e,m})) \quad , \quad \eta_{e,m} = e - 2 + 2(m-1)/(M_p + M_s) \tag{19}$$

where g is a one to one mapping from the set of integers $(e, m, n) \in [1, 2] \times [1, (M_p + M_s)/2] \times [1, N]$ to the single set $i \in [1, N_d/2]$. Here, we assume that $(M_p + M_s)$ is an even integer. In other cases (if needed), it only requires a slight modification of the distribution (19). We can note that the particular case $M_p = M_s = 1$ corresponds to the natural nodes of the quadratic interpolation. Now, for sake of clarity, we call $\boldsymbol{b}(\boldsymbol{x})$ the right hand side function in (3). Using the general expression (15), the collocation of (3) at a point $\boldsymbol{x}_i$ reads as follows

$$\begin{aligned}
\sum_{j=1}^{N^p_d} \left\{ \frac{1}{2}\boldsymbol{q}^p_j(\boldsymbol{x}_i) + \int_\Gamma \boldsymbol{T}(\boldsymbol{x}_i, \boldsymbol{y}) \boldsymbol{q}^p_j(\boldsymbol{y})\, d\Gamma_y \right\} u^p_j \quad + \\
\sum_{j=1}^{N^s_d} \left\{ \frac{1}{2}\boldsymbol{q}^s_j(\boldsymbol{x}_i) + \int_\Gamma \boldsymbol{T}(\boldsymbol{x}_i, \boldsymbol{y}) \boldsymbol{q}^s_j(\boldsymbol{y})\, d\Gamma_y \right\} u^s_j \quad = \quad \boldsymbol{b}(\boldsymbol{x}_i)
\end{aligned} \tag{20}$$

Now, we define the following matrix coefficients

$$W^\alpha_{2(i-1)+\beta,j} = \boldsymbol{e}_\beta \cdot \boldsymbol{q}^\alpha_j(\boldsymbol{x}_i)\,, \tag{21}$$

$$T^\alpha_{2(i-1)+\beta,j} = \boldsymbol{e}_\beta \cdot \int_\Gamma \boldsymbol{T}(\boldsymbol{x}_i, \boldsymbol{y}) \boldsymbol{q}^\alpha_j(\boldsymbol{y})\, d\Gamma_y\,, \tag{22}$$

$$b_{2(i-1)+\beta} = \boldsymbol{e}_\beta \cdot \boldsymbol{b}(\boldsymbol{x}_i)\,, \tag{23}$$

where the superscript α stands for the symbols p and s and $\beta = 1, 2$ corresponds to the horizontal (resp. vertical) component. The system (20) can be written in its matrix form

$$\boldsymbol{A}\boldsymbol{u} = \begin{pmatrix} \boldsymbol{A}^p & \boldsymbol{A}^s \\ \boldsymbol{T}_0^p & \boldsymbol{T}_0^s \end{pmatrix} \begin{pmatrix} \boldsymbol{u}^p \\ \boldsymbol{u}^s \end{pmatrix} = \boldsymbol{b}. \tag{24}$$

where $\boldsymbol{A}^\alpha$ is the $N_d \times N_d^\alpha$ rectangular matrix,

$$\boldsymbol{A}^\alpha = \frac{\boldsymbol{W}^\alpha}{2} + \boldsymbol{T}^\alpha, \tag{25}$$

and $\boldsymbol{T}_0^\alpha$ is a $2N_0 \times N_d^\alpha$ rectangular matrix. Here again, α stands for the symbols p and s. The matrix $\boldsymbol{T}_0^\alpha$ corresponds to the additional zero displacement conditions when collocating (4) at the N_0 CHIEF points. We can observe that when returning to the conventional approach (i.e. $M_p = M_s = 1$ with the quadratic polynomial basis (16,17)), the system (24) reduces to the well known '$\boldsymbol{H}$' BEM matrix [6]. The only difference here, is that the geometry of the curve Γ is not discretized with the aid of the quadratic shape functions as is commonly the case in traditional BEM. In our numerical sheme, the *real* curve is considered in the computation of the element matrices. The Cauchy principal value of singular integrals involved in (22) are performed using the procedure developed by Guiggiani and Casalini [9]. These singular integrals stem from the off-diagonal terms of the traction tensor and are of the type

$$I = \int_{\Gamma_n} T_{12}(\boldsymbol{x}_i, \boldsymbol{y}) \boldsymbol{q}_j^\alpha(\boldsymbol{y}) \cdot \boldsymbol{e}_2 \, d\Gamma_y$$

and similarly for T_{21}. Now, let $\bar{\eta}$ be the local coordinate of $\boldsymbol{x}_i$. This integral can be transformed into a non singular integral as

$$I = \int_{-1}^{+1} \frac{\boldsymbol{e}_2}{\eta - \bar{\eta}} \cdot \left\{ T_{12}(\boldsymbol{x}_i, \boldsymbol{y}(\eta)) \boldsymbol{q}_j^\alpha(\boldsymbol{y}(\eta)) J^n(\eta)(\eta - \bar{\eta}) - \frac{\boldsymbol{q}_j^\alpha(\boldsymbol{x}_i)\kappa^2}{2\pi} \right\} d\eta + \frac{\boldsymbol{e}_2 \cdot \boldsymbol{q}_j^\alpha(\boldsymbol{x}_i)\kappa^2}{2\pi} R(\bar{\eta})$$

where J^n is the Jacobian of the geometric transformation (9). The coefficient $\kappa^2/2\pi$ stems from the asymptotic behaviour of T_{12} when $\boldsymbol{y}$ approaches $\boldsymbol{x}_i$ along the boundary. The function $R(\bar{\eta})$ has the following expression

$$\begin{aligned} R(\bar{\eta}) &= \ln \frac{|1 - \bar{\eta}|}{|1 + \bar{\eta}|} \quad , \quad |\bar{\eta}| \neq 1 \\ R(\bar{\eta}) &= -\bar{\eta} \ln 2 \quad , \quad |\bar{\eta}| = 1. \end{aligned}$$

The weak singularity contained in the right-hand side of (3) is efficiently handled by using the cubic Telles' transformation [15]. All operations are performed with double precision and the Stokes' traction tensor terms are evaluated using the routines for Bessel functions of fractional order from Numerical Recipes [16]. In order to keep a good accuracy when computing these terms for very small argument (typically $k_s|\boldsymbol{x} - \boldsymbol{y}| < 10^{-4}$), asymptotic formulas derived from the series expansion given in Abramovitz *et al.* [17] are used. The overdetermined system then is solved by a standard Singular Value Decomposition routine. Because the plane wave basis (10) can give rise to numerical instabilities manifested in highly ill-conditioned matrices, small singular values below $10^{-12}\sigma_1$ (σ_1 denotes the biggest singular value) are discarded in order to avoid round-off errors and to achieve a better accuracy.

5. RESULTS

5.1. Harmonic waves from a circular cavity

Suppose we have an infinite cylindrical cavity of radius a in an elastic medium. On the cavity surface, we consider a prescribed traction $\boldsymbol{t}$ of the form

$$\boldsymbol{t} = p_0 \boldsymbol{e}_r + \sigma_0 \boldsymbol{e}_\theta \,, \tag{26}$$

where $(\boldsymbol{e}_r, \boldsymbol{e}_\theta)$ denotes the usual polar basis of the plane. Physically, this can be interpreted as a uniform harmonically varying pressure p_0 and a purely shear stress σ_0 acting on the cavity surface. The analytical solution for the displacement on the boundary is given in [18]:

$$\boldsymbol{u} = \left(\frac{p_0 a}{\mu}\right) \frac{\kappa_p H_0'(\kappa_p)}{\kappa_p^2 H_0(\kappa_p) + 2\kappa_p H_0'(\kappa_p)} \cdot \boldsymbol{e}_r + \left(\frac{\sigma_0 a}{\mu}\right) \frac{\kappa_s H_0'(\kappa_s)}{\kappa_s^2 H_0(\kappa_s) + 2\kappa_s H_0'(\kappa_s)} \cdot \boldsymbol{e}_\theta \,, \tag{27}$$

where κ_p (resp. κ_s) stand for the non-dimensional wavenumber $k_p a$ (resp. $k_s a$). H_0 denotes the Hankel function of the first kind of zero order and prime denotes differentiation with respect to the argument. In the sequel, we simplify the previous expression by taking $\mu = p_0 a = \sigma_0 a$. In all cases, the compressional and shear wave numbers are chosen accordingly such that $k_s/k_p = 2$ which is a common value for a wide range of materials. This is purely for convenience, and is not a restriction of the method.

The circular cylinder is discretized with N elements given by the regular parametrization

$$\Gamma_n = \left\{ a(\cos\theta, \sin\theta) \quad , \quad \theta = \frac{\pi}{N}(2n - 1 + \eta) \quad , \quad \eta \in [-1, +1] \right\}. \tag{28}$$

In Figure 2 are plotted the radial and tangential displacements obtained numerically by using $M_p = M_s = 32$ directions with only 2 elements. Comparison with the analytical formula shows very good agreement and the ability for this new oscillatory basis to represent a constant profile with very good accuracy. The discrepancies observed when $k_s a > 40$ simply stems from a lack of degree of freedom in this frequency range.

5.2. Scattering by a circular cavity

We shall present some results concerning the scattering of an S-wave travelling from the left to the right along the horizontal direction,

$$\boldsymbol{u}^I(\boldsymbol{x}) = -\boldsymbol{e}_2 \exp[\mathrm{i} k_s \, \boldsymbol{e}_1 \cdot \boldsymbol{x}] \tag{29}$$

impinging a circular cavity of radius a. Here again, we took $k_s/k_p = 2$. This problem has an analytical solution that has been established by Pao [19].

The discretization of the cavity boundary is strictly the same as the one of the previous section (equ. (28)) and 10 zero displacement equations are added to alleviate the non-uniquenes problem. The quality of the solution is controlled by the relative L_2 error defined as

$$E_2 = \frac{\|\boldsymbol{u} - \tilde{\boldsymbol{u}}\|_{L_2(\Gamma)\times L_2(\Gamma)}}{\|\tilde{\boldsymbol{u}}\|_{L_2(\Gamma)\times L_2(\Gamma)}} \,, \tag{30}$$

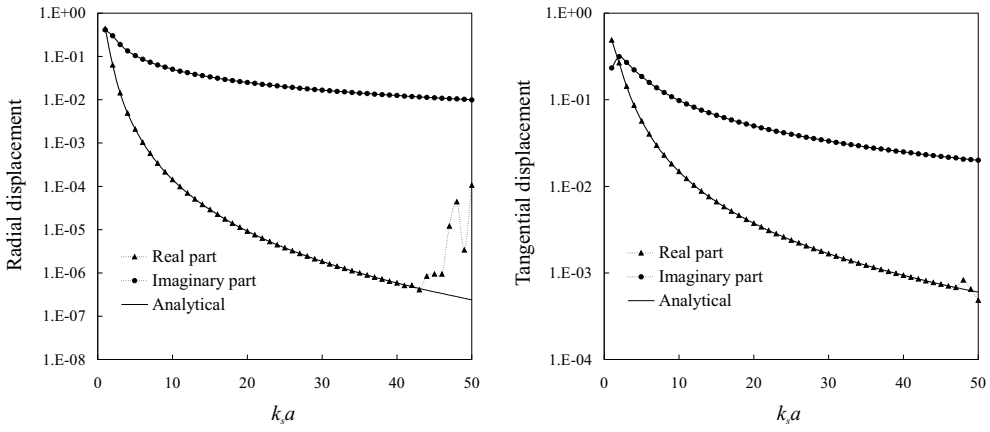

Figure 2. Displacement curve with respect to the frequency for the configuration: 2 wave elements with $M_p = M_s = 32$ directions. Computed values are taken at the mid-node of the first element.

where $\boldsymbol{u}$ and $\tilde{\boldsymbol{u}}$ denote the computed and exact solutions respectively. In Figure 3 are plotted the errors obtained for various configurations in the range of frequencies $0 \leq k_s a \leq 100$. The total number of variables for all these tests is kept constant with

$$N_d = 2N(M_p + Ms) = 432 \text{ (plane wave basis)} \quad \text{and} \quad N_d = 4N = 432 \text{ (quadratic)}.$$

The striking result is that the wave elements can produce errors up to *6 orders of magnitude* smaller than those of the conventional quadratic elements. This figure is also useful in terms of assessing the frequency range over which the two methods can provide reasonable accuracy (say 1% of relative error). It is clear that the conventional elements are sufficiently accurate up to $k_s a = 20$ and this corresponds to about 11 nodes per wavelength (we consider the smallest wavelength: $2\pi/k_s$). However, the new method can extend the useful frequency range to perhaps four times that value. Comparison between these numerical tests suggests that best results are obtained when considering large elements with many directions, the same effect was indeed observed for the Helmholtz equation [5].

In Table I are displayed errors obtained with $M_p = M_s = 36$ at high frequency. The number of elements is chosen such that the number of unknowns per wavelength is kept constant (about 3.6). 50 internal equations are considered here to ensure that the quality of the solution is not affected by the non-uniqueness problem. In this frequency range, the use of the quadratic interpolation would demand at least 5 times more variables if similar results are sought and this is above our current computational resources. In Figure 4 is displayed the real part of both radial and tangential displacements around the upper half of the circular cavity at $k_s a = 200$. The analytical solution perfectly matches with the computed one, to within the accuracy of the plot, and is therefore omitted here. Each element corresponds to an angular sector of 36°. They contain about twenty oscillations.

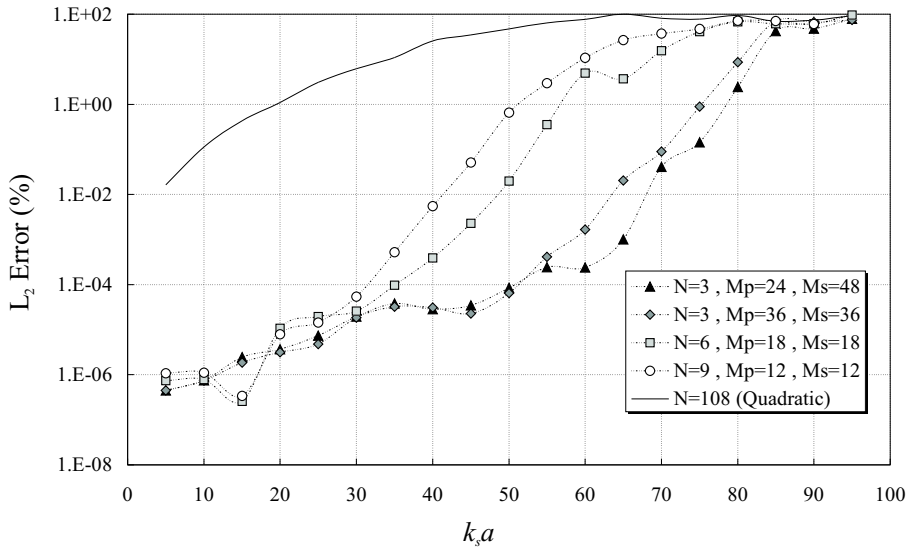

Figure 3. Error analysis for a incident S-wave scattered by a circular cavity of radius a.

$k_s a$	$E_2(\%)$	Wave elements	Unknowns
80	0.002	4	576
120	0.02	6	864
160	0.02	8	1152
200	0.045	10	1440

Table I. Relative L_2 errors (%) for high-frequency scattering of a S-wave by a circular cavity. $M_p = M_s = 36$.

6. CONCLUSIONS

The results clearly demonstrate that the plane wave basis formulation for boundary elements works as well for elastic wave scattering problems as it did for the Helmholtz equation. The overall properties of the method are essentially the same for the two types of problem. That is, for a given frequency, and the same number of degrees of freedom, the plane wave basis elements have errors which are orders of magnitude smaller than those for conventional boundary elements. Alternatively, if a given level of error is sought in the results, then far fewer degrees of freedom can be used. The above conclusions have been drawn from results from a small range of classical problems, but there is no reason to suppose that these findings are not quite general. In this regard, the present approach should be extended in order to take more general boundary conditions into account such as a prescribed velocity while the traction

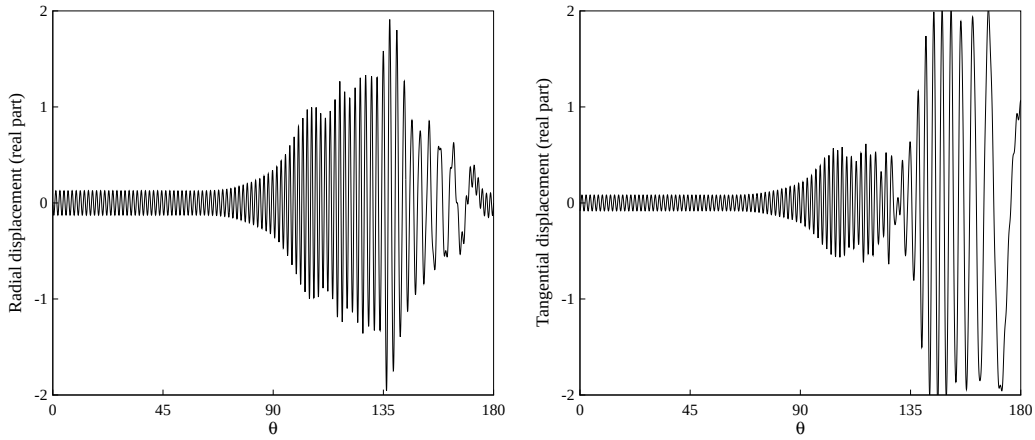

Figure 4. Displacement curve around the upper half of the circular cavity due to the scattering of a S-wave at $k_s a = 200$.

is kept unknown. This deserves further investigation, which is continuing.

Plane wave basis boundary elements have recently been applied to the three dimensional form of the Helmholtz equation [20], with great success, and so it may be conjectured that they can be applied to three dimensional problems of elastodynamics. Maxwell's electromagnetic equations are vector wave equations, of a similar form to those of elastodynamics. The chief difference is that all the electromagnetic waves propagate at the same speed, which, if anything, simplifies the problem. For this reason the authors believe that the methods presented here are equally applicable to scattering of electromagnetic waves governed by Maxwell's equations.

The remaining challenges are to make the integrations of the element matrices faster and more efficient, and to see if the plane wave basis boundary element equations can be solved using fast iterative methods. One unexplored possibility is the use of these plane wave basis boundary elements in conjunction with the Fast Multipole Method [21] and other recently developed rapid methods for short wave scattering [22].

ACKNOWLEDGEMENTS

This work has been funded by the EPSRC, under grant GR/N09879. We are very grateful to EPSRC for this support for Dr. Emmanuel Perrey-Debain. Peter Bettess is also grateful to the EPSRC Senior Research Fellowship committee, chaired by Professor Sir Richard Brook, which is funding this work, through EPSRC Grant Number: SF/000169.

REFERENCES

1. Melenk JM, Babuška I. The Partition of Unity Method. *Int. Journ. Num. Meth. Eng.*, 1997; **40**:727-758.
2. de La Bourdonnaye A. Convergence of the approximation of wave functions by oscillatory functions in the high frequency limit. *Comptes Rendus de l'Academie des Science. Paris.* Série I, 1994; **318**:765-768.

3. Perrey-Debain E, Trevelyan J, Bettess P. New special wave boundary elements for short wave problems. *Comm. Num. Meth. Eng.*, 2002; **18**(4):259-268.
4. Perrey-Debain E, Trevelyan J, Bettess P. Plane wave interpolation in direct collocation boundary element method for radiation and wave scattering: numerical aspects and applications. *J. Sound Vib.*, 2003; to appear.
5. Perrey-Debain E, Trevelyan J, Bettess P. Using wave boundary elements in BEM for high frequency scattering. *Proceedings of the Third UK Conference on Boundary Integral Methods*, University of Brighton, pp. 119 - 128, 2001.
6. Brebbia CA, Telles JCF, Wrobel LC. *Boundary Element Technique. Theory and Applications in Engineering*. Springer-Verlag, Berlin Heidelberg New York Tokyo, 1984.
7. Rizzo FJ, Shippy DJ, Rezayat M. A boundary integral equation method for radiation and scattering of elastic waves in three dimensions. *Int. Journ. Num. Meth. Eng.*, 1985; **21**:115-129.
8. Dominguez J. *Boundary Elements in Dynamics*. Computational Mechanics Publications, 1993.
9. Guiggiani M, Casalini P. Direct computation of Cauchy principal value integrals in advanced boundary elements. *Int. Journ. Num. Meth. Eng.*, 1987; **24**:1711-1720.
10. Amini S, Kirkup M. Solution of Helmholtz equation in the exterior domain by elementary boundary integral methods. *J. Comp. Phys.*, 1995; **118**:208-221.
11. Schenck HA. Improved integral formulation for acoustic radiation problems. *Journal of the Acoustical Society of America*, 1968; **44**:41-58.
12. Achenbach JD. *Wave Propagation in Elastic Solids*. Elsevier Science Publisher, 1984.
13. Beslin O, Nicolas J. A hierarchical functions set for predicting very high order plate bending modes with any boundary conditions. *J. Sound and Vib.*, 1997; **202**(5):633-655.
14. Leung AYT, Chan JKW. Fourier p-element for the analysis of beams and plates. *J. Sound and Vib.*, 1998; **212**(1):179-185.
15. Telles JCF. A self-adaptive co-ordinate transformation for efficient numerical evaluation of general boundary element integrals. *Int. Journ. Num. Meth. Eng.*, 1987; **24**:959-973.
16. Press WH, Teukolsky AA, Vetterling WT, Flannery BP. *Numerical Recipes in Fortran*, Cambridge University Press, 1992.
17. Abramovitz M, Stegun IA. *Handbook of Mathematical Functions*, Vol. 55 of Appl. Math. Ser., 10th edition, National Bureau of Standards, U.S. Governement Printing Office, Washington, D.C., 1972.
18. Graff KF. *Wave Motion in Elastic Solids*, Ohio State University Press, 1975.
19. Pao Y. Dynamical stress concentration in an elastic plate. *Transactions of the ASME, Ser. E - Journal of Applied Mechanics*, 1962; **29**(2):299-305.
20. Bettess P. Plane wave basis finite elements and boundary elements for scattering problems. *LMS Durham Symposium: Computational methods for wave propagation in direct scattering*, 15-25 July 2002, Durham University, U.K., URL:http://www.maths.strath.ac.uk/durham02.
21. Darve E. The fast multipole method: numerical implementation. *Journal of Computational Physics*, 2000; **1608**:195-240.
22. Bruno OP, Kunyansky LA. Surface scattering in three dimensions: an accelerated high-order solver. *Proceedings of the Royal Society of London Serie A*, 2001; **457**:1-14.

Appendix

Stokes tensors The Stokes' displacement tensor components U_{ij} referred to a cartesian basis are (see [8])

$$U_{ij}(\boldsymbol{x},\boldsymbol{y}) = \frac{1}{2\pi\mu}\left(\psi(r)\,\delta_{ij} - \chi(r)\frac{\partial r}{\partial y_i}\frac{\partial r}{\partial y_j}\right) \quad , \quad r = |\boldsymbol{x}-\boldsymbol{y}| \tag{31}$$

The Stokes' traction tensor components T_{ij} referred to a cartesian basis are given by

$$\begin{aligned} T_{ij}(\boldsymbol{x},\boldsymbol{y}) &= \frac{1}{2\pi}\left(\frac{d\psi}{dr} - \frac{\chi}{r}\right)\left(\delta_{ij}\frac{\partial r}{\partial n} + \frac{\partial r}{\partial y_j}n_i\right) \\ &- \frac{\chi}{\pi r}\left(\frac{\partial r}{\partial y_i}n_j - 2\frac{\partial r}{\partial y_i}\frac{\partial r}{\partial y_j}\frac{\partial r}{\partial n}\right) \\ &- \frac{1}{\pi}\frac{d\chi}{dr}\frac{\partial r}{\partial y_i}\frac{\partial r}{\partial y_j}\frac{\partial r}{\partial n} \\ &+ \frac{1}{2\pi}\left(\frac{k_s^2}{k_p^2} - 2\right)\left(\frac{d\psi}{dr} - \frac{d\chi}{dr} - \frac{\chi}{r}\right)\frac{\partial r}{\partial y_i}n_j \end{aligned} \tag{32}$$

where the normal derivative is taken at $\boldsymbol{y}$ and n_i are the components of the inward unit normal vector (see Figure 1). ψ and χ are the two radial functions defined as follows

$$\psi(r) = \frac{\mathrm{i}\pi}{2}\left\{H_0(k_s r) + \frac{1}{k_s r}\left[-H_1(k_s r) + \kappa H_1(k_p r)\right]\right\} \tag{33}$$

$$\chi(r) = -\frac{\mathrm{i}\pi}{2}\left\{H_2(k_s r) - \kappa^2 H_2(k_p r)\right\} \tag{34}$$

in which H_n is the Hankel function of the first kind and order n.

Asymptotic formulas By using the series expansion for the modified Bessel functions given in Abramovitz *et al.* [17] , we arrive at the following asymptotic formulas:

$$\begin{aligned}\psi &= -\frac{1}{2}(\ln z_s + \kappa^2 \ln z_p) - \gamma + \frac{1-2\gamma}{4}(\kappa^2 - 1) - \ln z_s C(z_s) + B(z_s) \\ &\quad + \frac{1}{2}(\ln z_s D(z_s) - \kappa^2 \ln z_p D(z_p)) + \frac{1}{4}(\kappa^2 A(z_p) - A(z_s))\end{aligned} \tag{35}$$

$$\begin{aligned}\chi &= -\frac{1}{2}(1-\kappa^2) + \ln z_s (D(z_s) - C(z_s)) - \kappa^2 \ln z_p (D(z_p) - C(z_p)) \\ &\quad + B(z_s) - \frac{A(z_s)}{2} - \kappa^2\left(B(z_p) - \frac{A(z_p)}{2}\right)\end{aligned} \tag{36}$$

in which $z_p = -\mathrm{i}k_p r/2$, $z_s = -\mathrm{i}k_s r/2$ and γ is the Euler constant. These last expressions are only valid for $r \to 0$ while k_p, k_s are kept fixed. Functions A, B, C and D stand for the following complex series:

$$A(z) = \sum_{n=1}^{\infty} \frac{\psi(n+1) + \psi(n+2)}{n!(n+1)!}\, z^{2n} \tag{37}$$

$$B(z) = \sum_{n=1}^{\infty} \frac{\psi(n+1)}{(n!)^2}\, z^{2n} \tag{38}$$

$$C(z) = \sum_{n=1}^{\infty} \frac{1}{(n!)^2}\, z^{2n} \tag{39}$$

$$D(z) = \sum_{n=1}^{\infty} \frac{1}{n!(n+1)!}\, z^{2n} \tag{40}$$

where ψ is defined by $\psi(1) = -\gamma$ and

$$\psi(n) = -\gamma + \sum_{k=1}^{n-1} \frac{1}{k} \quad \text{for} \quad n \geq 2. \tag{41}$$

Asymptotic expressions for $d\psi/dr$ and $d\chi/dr$ are obtained by differentiating the corresponding formulas. In practice, the 4 or 5 first terms in the above infinite series have been found to be sufficient in our calculation.